Observation of pure inverse spin Hall effect in ferromagnetic metals via ferromagnetic/antiferromagnetic exchange-bias structures

H. Wu, C. H. Wan,[*] Z. H. Yuan, X. Zhang, J. Jiang, Q. T. Zhang, Z. C. Wen, and X. F. Han[†]

Beijing National Laboratory for Condensed Matter Physics, Institute of Physics, Chinese Academy of Sciences, Beijing 100190, China

We report that the spin current generated by the spin Seebeck effect (SSE) in yttrium iron garnet (YIG) can be detected by a ferromagnetic metal (NiFe). By using the ferromagnetic/antiferromagnetic (FM/AFM) exchange bias structure (NiFe/IrMn), the inverse spin Hall effect (ISHE) and planar Nernst effect (PNE) of NiFe can be unambiguously separated, allowing us to observe a pure ISHE signal. After eliminating the in-plane temperature gradient in NiFe, we can even observe a pure ISHE signal without PNE from NiFe itself. It is worth noting that a large spin Hall angle (0.098) of NiFe is obtained, which is comparable with Pt. This work provides a kind of FM/AFM exchange bias structure to detect the spin current by charge signals, and highlights that ISHE in ferromagnetic metals can be used in spintronic research and applications.

How to generate, manipulate, and detect spin currents (J_S) is a fundamental issue in spintronic research [1,2]. Spin injection from a ferromagnetic metal [3,4], spin pumping [5,6], the spin Hall effect (SHE) [7,8], and the spin Seebeck effect (SSE) [9–15] provide several ways to generate a spin current. Especially SSE in ferromagnetic insulators (FI) [11–14] has attracted much attention because a pure spin current can be generated without any charge flow. The inverse spin Hall effect (ISHE) [5,16] in heavy metals with strong spin-orbit coupling (SOC) such as Pt is often used to detect the spin current by charge signals: $E_{ISHE} = (\theta_{SH}\rho)J_S \times \sigma$, where E_{ISHE} is the ISHE electric field, θ_{SH} is the spin Hall angle, ρ is the resistivity, and σ is the unit vector of spin.

As the inverse effect of the anomalous Hall effect (AHE), ISHE in ferromagnetic metals provides a possibility to detect the spin current as well. Recently, several works focused on using ferromagnetic metals instead of metals with strong SOC to detect the spin current generated by SSE in FI [17–19]. However, additional anomalous Nernst effect (ANE) and planar Nernst effect (PNE) in the ferromagnetic metal itself is often mixed with the ISHE signal in longitudinal and transversal spin Seebeck measurements respectively. Therefore, in transversal spin Seebeck measurement, unambiguous separation of PNE and ISHE signals will be an important step, not only for exploring the physical mechanism of ISHE in ferromagnetic metals, but also for future applications in detecting spin currents.

The exchange-bias phenomenon in the ferromagnetic/antiferromagnetic (FM/AFM) interface [20,21] can provide a shift field (H_{EB}) of the magnetization hysteresis loop, when cooling down to Neel temperature (T_N) with a static magnetic field, which has been used in spin valve structures for several years. This phenomenon is associated with the interfacial exchange anisotropy between ferromagnetism and antiferromagnetism, and ferromagnetism tends to align parallel with uncompensated spins of antiferromagnetism at the interface. Therefore, ferromagnetism has a unidirectional anisotropy.

In this work, the NiFe/IrMn exchange bias structure has been employed to detect the spin current in NiFe originating from SSE in yttrium iron garnet (YIG); Cu was inserted between NiFe and YIG to decrease the exchange coupling and to eliminate the possible magnetic proximity effect [22,23]. The temperature gradient ∇T is mainly in plane and along the exchange bias field axis. However, PNE from NiFe itself will be involved in ISHE voltages [24,25]. This structure can separate the magnetization reversal process of YIG and NiFe. As a result, ISHE and PNE, which are related to the magnetization states of YIG and NiFe respectively, could be separated as well.

The detail multilayer film structure is GGG/YIG/Cu(t nm)/NiFe(5 nm)/IrMn(12 nm)/Ta(5 nm). First, a 3.5 μm YIG film was grown on a 300 μm GGG(111) substrate using the liquid phase epitaxial method. Then upper films were deposited using an ultrahigh vacuum magnetron sputtering system (ULVAC) at a pressure of 0.16 Pa and a power of 120 W. In order to provide a clear interface between YIG and Cu, the YIG surface was cleaned for 60 s by Ar plasma in the vacuum chamber before deposition. A 100 Oe magnetic field was applied during deposition, which could induce an easy magnetization axis and an exchange bias of NiFe. Films were patterned by photolithography combined with Ar ion etching. Both of the electrodes A and C are of 10 μm × 100 μm in size, and the size of electrode B is 50 μm × 100 μm ($L = 100$ μm). The spacing between A (B) and B (C) is 10 μm.

Figure 1(a) shows the schematic illustration of the measurement method. Electrodes A and C were used to heat the YIG film by electric currents I_H (Keithley 2440), which induced a transverse temperature gradient ∇T mainly along the y axis, and the heating power $P \propto I_H^2 \propto \nabla T$. Because of SSE in YIG, ∇T produces a spin accumulation at the interface between YIG and electrode B, and then the spin current is injected to electrode B. By measuring the voltage along the x axis in electrode B (Keithley 2182A), the spin current can be detected by means of ISHE, as shown in Fig. 1(b). The physical property measurement system (Quantum Design PPMS) was used to apply the magnetic field and control the temperature. All measurements were performed at room temperature.
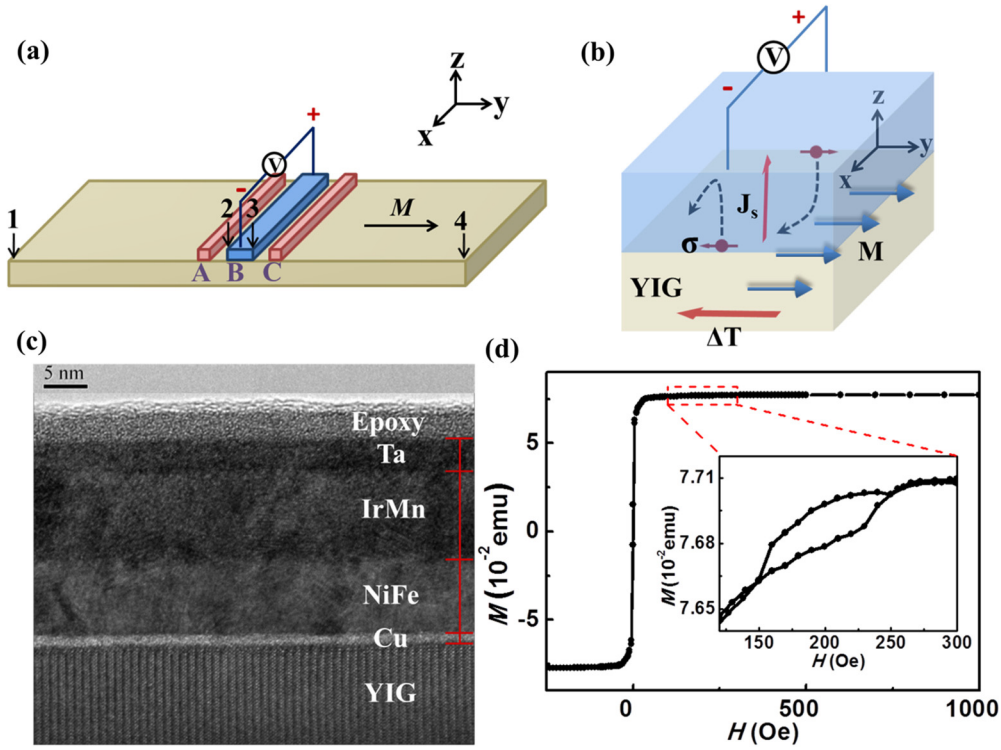
---

[*]wancaihua@iphy.ac.cn

[†]xfhan@iphy.ac.cn

FIG. 1. (Color online) (a) A schematic of patterned device structures. A and C electrodes are for heating currents I_H and the B electrode is for ISHE voltage V_{ISHE} measurement. (b) A schematic illustration of ISHE in electrode B induced by SSE in YIG. The temperature gradient ∇T is mainly along the y axis and the spin current in B is along the z axis, therefore the ISHE voltage is measured along the x axis. (c) Cross-section HRTEM results of the YIG/Cu(3 nm)/NiFe(5 nm)/IrMn(12 nm)/Ta(5 nm) sample for detecting the spin current. (d) M-H loops of the YIG/Cu(5 nm)/NiFe(5 nm)/IrMn(12 nm)/Ta(5 nm) sample; the magnetic field is along y axis.

The cross-section high resolution transmission electron microscopy (HRTEM) of the GGG/YIG/Cu(3 nm)/NiFe(5 nm)/IrMn(12 nm)/Ta(5 nm) sample was observed by a Tecnai G2 F20 S-TWIN (200 kV) system. HRTEM results are shown in Fig. 1(c). The high quality YIG single-crystal structure is formed on the GGG(111) substrate, and the epitaxial direction of the YIG film is also along the (111) direction. Four metal layers deposited by magnetron sputtering are continuous and flat, and each interface, especially the interface between YIG and Cu, is very clear and sharp. The spin current is injected from YIG to films above, so a clear YIG/Cu interface is very important.

The magnetic hysteresis loop of the GGG/YIG/Cu(5 nm)/NiFe(5 nm)/IrMn(12 nm)/Ta(5 nm) sample was measured by a vibrating sample magnetometer (VSM, MicroSense EZ-9) with magnetic field applied along the y axis (also the axis of the exchange bias field), as shown in Fig. 1(d). YIG is a very soft magnetic material and the saturation field (H_S) of YIG is less than 10 Oe. The inset figure shows the minor M-H loop from NiFe, and H_{EB} (200 Oe) is enough to distinguish the magnetization reversals of NiFe and YIG. Besides, the magnetic moment from YIG is very large due to its larger thickness.

As reported in previous works [9–14], first we used a 10 nm thick (d_{Pt}) Pt film to detect J_S induced by SSE in YIG. A 300 nV ISHE voltage is observed as $I_H = 10$ mA in electrode C is applied with field along the y axis [Fig. 2(a)]. ISHE voltages were not observed when the field was applied along the x and z axes, which confirms the SSE scenario. When a 3 nm metal Cu

layer is inserted between Pt and YIG to eliminate the magnetic proximity effect between YIG and Pt, still a spin current can pass without remarkable dissipation, as proven by the ISHE voltage observed in this case. However, once a 3 nm insulator MgO layer is inserted to block J_S from YIG, the ISHE voltage completely disappears. These results confirm that the voltage is induced by J_S injected from YIG. This voltage does not come from Pt or YIG alone, which could be proven by the absence of the voltage in YIG/Cu and Si-SiO$_2$/Pt reference samples.

When we changed the heating electrode from C to A, $T_{B,A}$, $T_{1,A}$, $T_{4,A}$ and $T_{B,C}$, $T_{1,C}$, $T_{4,C}$ represent the temperatures of points B, 1, 4 when heating A and C respectively; $T_{B,A+C}$, $T_{1,A+C}$, and $T_{4,A+C}$ represent the temperatures of points B, 1, and 4 when heating A and C simultaneously. $T_{1,C} = T_{4,A}$, $T_{B,A} = T_{B,C}$, and $T_{1,A+C} = T_{4,A+C}$ due to the geometrical symmetry. So the ISHE voltage $V_{ISHE,A} = S_1(T_{B,A} - T_{4,A}) = V_{ISHE,C} = S_1(T_{B,C} - T_{1,C})$, where $S_1 = \frac{1}{2}\theta_{Pt}\eta_{YIG-Pt}(L_{Pt}/d_{Pt})S_S$, θ_{Pt} is the spin Hall angle of Pt, η_{YIG-Pt} is the spin injection efficiency, L_{Pt}/d_{Pt} is the aspect ratio and S_S is the spin Seebeck coefficient [9]. The ISHE voltage is almost the same when changing the heating electrode from C to A, as shown in Fig. 2(b). When heating A and C at the same time, the ISHE voltage is enhanced due to higher temperature gradient: $V_{ISHE,A+C} = S_1(T_{B,A+C} - T_{4,A+C}) = S_1(T_{B,A+C} - T_{1,A+C})$ [Fig. 2(b)].

We also measured the V_{ISHE}-I_H curves with fields along the y axis larger than H_S of YIG (± 20 Oe) and then obtained the difference between them, namely spin dependent ISHE
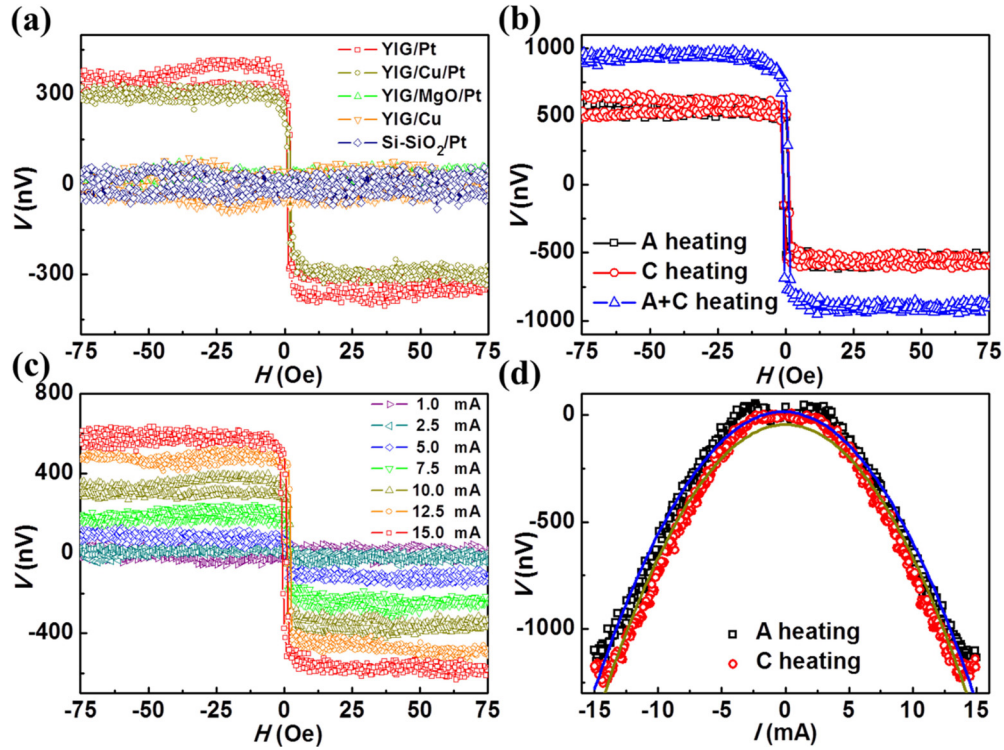
FIG. 2. (Color online) (a) H dependence of V_{ISHE} in YIG/Pt(10 nm), YIG/Cu(3 nm)/Pt(10 nm), YIG/MgO(3 nm)/Pt(10 nm), YIG/Cu(10 nm), and Si-SiO$_2$/Pt(10 nm) samples. (b) H dependence of V_{ISHE} for heating A or C respectively, and simultaneously heating A and C in the YIG/Pt(10 nm) sample. (c) H dependence of V_{ISHE} for different I_H in electrode C in the YIG/Pt(10 nm) sample. (d) I_H dependence of V_{ISHE} and fitting curves for heating A or C in the YIG/Pt(10 nm) sample.

voltages: $V_{ISHE} = V(+M_s) - V(-M_s)$. Figures 2(c) and 2(d) show the relationship between ISHE voltages and heating currents: $V_{ISHE} \propto I_H^2 \propto \nabla T$, which confirms that the ISHE signal is thermal related. Also the V_{ISHE}-I_H curves nearly coincide after changing the heating electrode from C to A.

Furthermore, we changed the spin current detector Pt with the exchange bias structure, Cu(5 nm)/NiFe(5 nm)/IrMn(12 nm)/Ta(5 nm), and heated the electrode C with $I_H = 15$ mA. The heating current generates ∇T not only in YIG, but also in electrode B, which induces a PNE voltage in NiFe. By using the exchange bias structure, magnetization reversals of NiFe and YIG are separated, as can be seen in Fig. 1(d). As a result, ISHE (related to magnetization of YIG) and PNE (related to magnetization of NiFe) are separated as well. As shown in Fig. 3(a), a 500 nV PNE voltage is observed and the center field of the PNE curve locates at 120 Oe. This shift field is smaller than the H_{EB} from M-H curves for two reasons: one is that the film is patterned, and another is that the temperature of the electrode B increases when heating C.

It is especially attractive that a 250 nV V_{ISHE} is observed near zero magnetic field and the voltage saturates at a field less than 10 Oe, which is similar to the signal in the YIG/Pt sample. Also the sign of the ISHE voltage in NiFe is the same as that in Pt. Transport properties only depend on the magnetization of NiFe, because YIG is an insulator. Anisotropic magnetoresistance (AMR) and planar Hall effect (PHE) reflect the magnetization state of NiFe and share the similar origin with PNE. AMR and PHE only have signals near 150 Oe, and do not have obvious signals near 0 Oe. Especially

PHE almost has the same curve as PNE; the only difference is that one is from the electric current, and the other is from the thermal current. These prove that the signal near 0 Oe is not from PNE in NiFe, but from ISHE in NiFe induced by SSE in YIG, which can also be confirmed by M-H curves in Fig. 1(d).

When the thickness of inserted Cu varies from 3 to 10 nm, three changes emerge as follows: (1) V_{ISHE} decreases gradually and even disappears due to increased spin relaxation in Cu [26] and decreased resistance of electrode B; (2) V_{PNE} decreases because the temperature gradient ∇T in NiFe also decreases; (3) H_{EB} of NiFe increases with thicker Cu because the exchange coupling between NiFe and YIG weakens. On the other hand, once a 3 nm insulator MgO layer is inserted, V_{ISHE} disappears while V_{PNE} still exists under the same precision, as shown in Fig. 3(b), because thermal currents can still conduct even in insulators, but spin currents cannot. These results also confirm that the signal near 0 Oe is not from NiFe itself, as ANE or PNE.

$T_{B2,A}$, $T_{B3,A}$ and $T_{B2,C}$, $T_{B3,C}$ represent the temperatures of boundaries 2, 3 of electrode B when heating electrodes A and C respectively; $T_{B2,A+C}$, $T_{B3,A+C}$ represent the temperatures of boundaries 2, 3 of electrode B when heating A and C simultaneously. Due to the geometrical symmetry, $T_{B2,A} = T_{B3,C}$, $T_{B3,A} = T_{B2,C}$, $T_{B2,A+C} = T_{B3,A+C}$. V_{ISHE} and V_{PNE} voltages satisfy the following equations: $V_{ISHE,A} = S_2(T_{B,A} - T_{4,A}) = V_{ISHE,C} = S_2(T_{B,C} - T_{1,C})$, where $S_2 = \frac{1}{2}\theta_{NiFe}\eta_{YIG\text{-}Cu\text{-}NiFe}(L_{NiFe}/d_{NiFe})S_S$; $V_{PNE,A} = N(\boldsymbol{M})(T_{B2,A} - T_{B3,A}) = -V_{PNE,C} = -N(\boldsymbol{M})(T_{B2,C} - T_{B3,C})$, where $N(\boldsymbol{M})$ is the simplified coefficient. When changing the heating
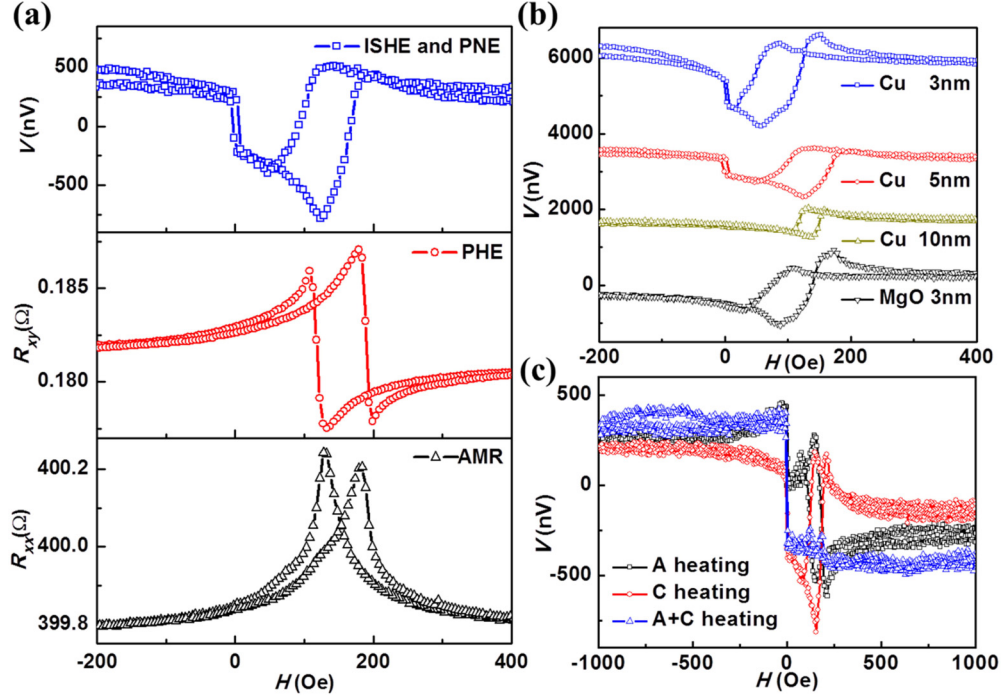
FIG. 3. (Color online) (a) H dependence of ISHE, PNE, AMR, and PHE signals in the YIG/Cu(5 nm)/NiFe(5 nm)/IrMn(12 nm)/Ta(5 nm) sample. (b) H dependence of V_{ISHE} and V_{PNE} in YIG/x/NiFe(5 nm)/IrMn(12 nm)/Ta(5 nm) samples with different inserted layers $x =$ Cu 3 nm, Cu 5 nm, Cu 10 nm, and MgO 3 nm. (c) H dependence of V_{ISHE} and V_{PNE} for heating A or C respectively, and simultaneously heating A and C in the YIG/Cu(5 nm)/NiFe(5 nm)/IrMn(12 nm)/Ta(5 nm) sample.

electrode from C to A, V_{PNE} is opposite in sign, while V_{ISHE} is the same, as shown in Fig. 3(c). When heating A and C at the same time, $V_{ISHE,A+C} = S_2(T_{B,A+C} - T_{4,A+C}) = S_2(T_{B,A+C} - T_{1,A+C})$, $V_{PNE,A+C} = N(\boldsymbol{M})(T_{B2,A+C} - T_{B3,A+C}) = 0$. By eliminating ∇T along y axis in NiFe, V_{PNE} in NiFe could nearly be canceled, while V_{ISHE} is enhanced because of the enhanced ∇T in YIG. In this way, we succeed in directly detecting the pure V_{ISHE} in NiFe without the influence of V_{PNE} from NiFe itself [Fig. 3(c)]. Besides, ∇T along the z axis in NiFe will be also enhanced when simultaneously heating A and C. Even in this case, ANE voltages in NiFe are not observed, indicating that ∇T along the z axis in NiFe is negligibly small.

To further illustrate ISHE in NiFe, we measured the I_H dependence of V_{ISHE} and V_{PNE}, as shown in Fig. 4. The center field of the PNE curve corresponds to H_{EB} of NiFe, and it decreases with increasing I_H, as shown in Fig. 4(a), because H_{EB} in the FM/AFM structure usually decreases with increasing temperature, and even drops to zero at blocking temperature.

Figures 4(c) and 4(d) show the I_H dependence of V_{PNE} [$V(+250$ Oe$)-V(+20$ Oe$)$] and V_{ISHE} [$V(+10$ Oe$)-V(-10$ Oe$)$] respectively; they are both proportional to I_H^2, confirming their thermal dependence. V_{PNE} is opposite in sign when we changed the heating electrode from C to A, while V_{ISHE} remains unchanged. This difference also confirms that these two signals should come from different origins: one from PNE in NiFe, and another from ISHE in NiFe induced by SSE in YIG. By simultaneously heating A and C, as shown in Fig. 4(e), enhanced pure V_{ISHE} is observed, while V_{PNE} from NiFe itself is totally eliminated.

To quantitatively analyze the spin Hall angle θ_{SH} of NiFe, we measured the P dependence of V_{ISHE} in YIG/Pt(10 nm) and YIG/Cu(5 nm)/NiFe(5 nm)/IrMn(12 nm)/Ta(5 nm) samples, as shown in Fig. 4(f). ISHE induced charge currents, $V_{ISHE}/R = \beta\theta_{SH}P$, where R is the resistance of electrode B. We suppose the coefficient β that expresses the efficiency from thermal currents to spin currents in electrode B is the same in these two samples. By linear fitting V_{ISHE}/R-P curves, the relative spin Hall angle $\theta_{SH}(NiFe)/\theta_{SH}(Pt) \approx 0.98$. By using $\theta_{SH}(Pt) = 0.1$ [27], we obtain $\theta_{SH}(NiFe) = 0.098$, which is at the same order as $\theta_{SH}(NiFe) = 0.02$ measured by spin pumping [28]. These results show that NiFe almost has a spin Hall angle comparable to Pt. In fact, previous works have suggested strong SOC in 3d transition metals [29,30] and connected ISHE with AHE in a ferromagnetic metal (CoFeB) through the Mott relation [19]. Strong SOC and ferromagnetic order in NiFe should contribute to the large θ_{SH}. By using the exchange bias structure, investigating SHE and ISHE in ferromagnetic metals will become more feasible. As heavy metals with strong SOC, ferromagnetic metals become another promising candidate for detecting spin currents.

In conclusion, first a spin current in NiFe is generated by SSE in YIG, and then is detected by charge signals due to ISHE. The NiFe/IrMn exchange bias structure was used to separate ISHE and PNE in NiFe, and inserted Cu can decouple the exchange coupling and rule out the possible magnetic proximity effect between NiFe and YIG, allowing us to observe a pure ISHE signal. By simultaneously heating electrodes on both sides of electrode B, which can eliminate the in-plane temperature gradient in
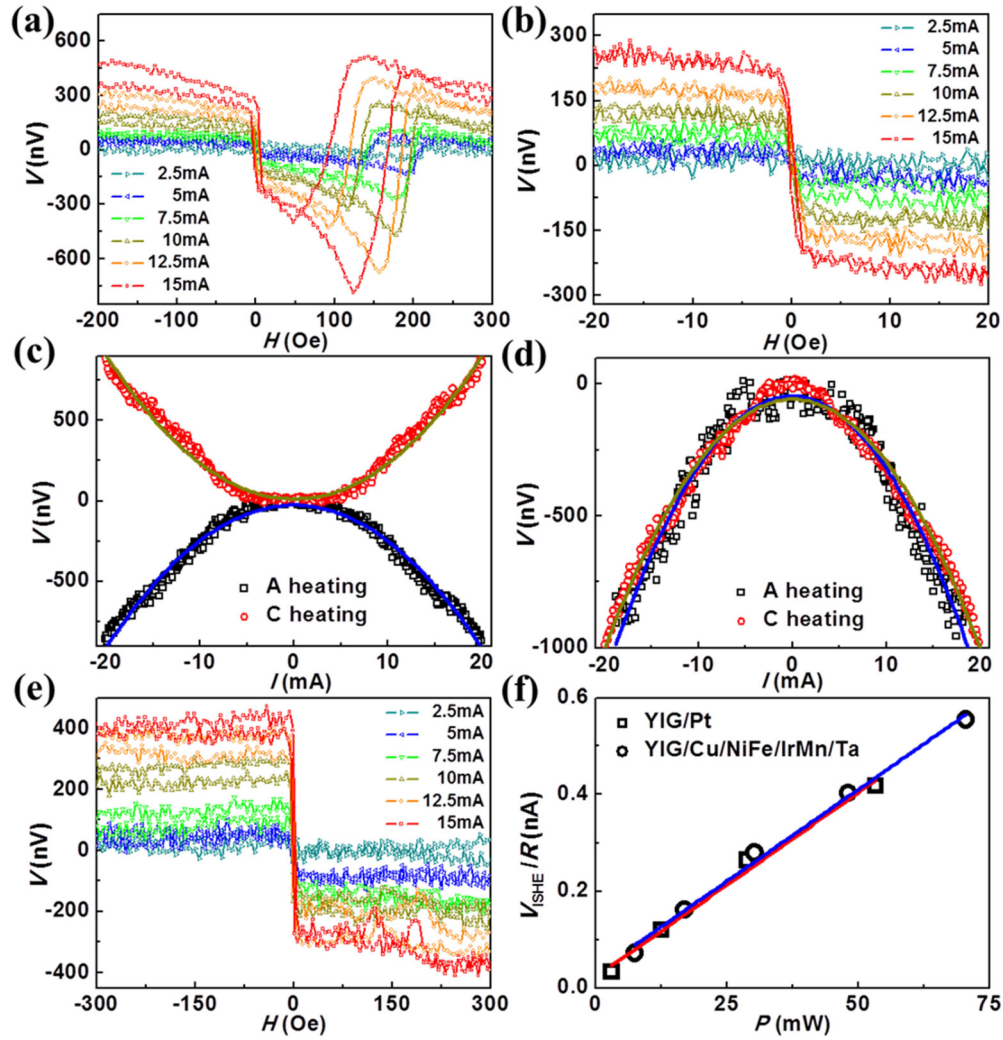
FIG. 4. (Color online) (a)–(e) were measured in the YIG/Cu(5 nm)/NiFe(5 nm)/IrMn(12 nm)/Ta(5 nm) sample. We used the magnetic field ranges ±1000 Oe and ±50 Oe to measure the signal in (a) and (b) respectively. Panel (a) shows the H dependence of V_{ISHE} and V_{PNE} for different I_H in electrode C, and (b) shows the pure H dependent V_{ISHE} due to the small field range. (c),(d) I_H dependence and fitting curves of V_{PNE} and V_{ISHE} for heating electrode A or C respectively. (e) H dependence of pure V_{ISHE} for different I_H in both electrodes A and C. (f) Heating power P dependence of V_{ISHE}/R in YIG/Pt(10 nm) and YIG/Cu(5 nm)/NiFe(5 nm)/IrMn(12 nm)/Ta(5 nm) samples.

NiFe, PNE from NiFe itself is eliminated, while only ISHE remains. By fitting the V_{ISHE}/R-P curves, we obtain a large spin Hall angle (0.098) in NiFe. This work is crucial to unambiguous confirmation of the existence of ISHE in ferromagnetic metals and also to the applications of FM-based ISHE.

[1] S. A. Wolf, D. D. Awschalom, R. A. Buhrman, J. M. Daughton, S. V. Molnar, M. L. Roukes, A. Y. Chtchelkanova, and D. M. Treger, Science **294**, 1488 (2001).

[2] I. Žutić, J. Fabian, and S. D. Sarma, Rev. Mod. Phys. **76**, 323 (2004).

[3] M. Johnson and R. H. Silsbee, Phys. Rev. Lett. **55**, 1790 (1985).

[4] F. J. Jedema, A. T. Filip, and B. J. van Wees, Nature (London) **410**, 345 (2001).

[5] E. Saitoh, M. Ueda, H. Miyajima, and G. Tatara, Appl. Phys. Lett. **88**, 182509 (2006).

[6] O. Mosendz, J. E. Pearson, F. Y. Fradin, G. E. W. Bauer, S. D. Bader, and A. Hoffmann, Phys. Rev. Lett. **104**, 046601 (2010).

[7] Y. K. Kato, R. C. Myers, A. C. Gossard, and D. D. Awschalom, Science **306**, 1910 (2004).

[8] S. O. Valenzuela and M. Tinkham, Nature (London) **442**, 176 (2006).

[9] K. Uchida, S. Takahashi, K. Harii, J. Ieda, W. Koshibae, K. Ando, S. Maekawa, and E. Saitoh, Nature (London) **455**, 778 (2008).

[10] G. E. W. Bauer, E. Saitoh, and B. J. van Wees, Nat. Mater. **11**, 391 (2012).

[11] K. Uchida, J. Xiao, H. Adachi, J. Ohe, S. Takahashi, J. Ieda, T. Ota, Y. Kajiwara, H. Umezawa, Kawai, G. E. W. Bauer, S. Maekawa, and E. Saitoh, Nat. Mater. **9**, 894 (2010).

[12] K. Uchida, H. Adachi, T. Ota, H. Nakayama, S. Maekawa, and E. Saitoh, Appl. Phys. Lett. **97**, 172505 (2010).

[13] K. Uchida, T. Nonaka, T. Ota, and E. Saitoh, Appl. Phys. Lett. **97**, 262504 (2010).

[14] P. Li, D. Ellsworth, H. Chang, P. Janantha, D. Richardson, F. Shah, P. Phillips, T. Vijayasarathy, and M. Wu, Appl. Phys. Lett. **105**, 242412 (2014).

[15] H. Adachi, K. Uchida, E. Saitoh, and S. Maekawa, Rep. Prog. Phys. **76**, 036501 (2013).

[16] T. Kimura, Y. Otani, T. Sato, S. Takahashi, and S. Maekawa, Phys. Rev. Lett. **98**, 156601 (2007).

[17] B. F. Miao, S. Y. Huang, D. Qu, and C. L. Chien, Phys. Rev. Lett. **111**, 066602 (2013).

[18] D. Tian, Y. F. Li, D. Qu, X. F. Jin, and C. L. Chien, Appl. Phys. Lett. **106**, 212407 (2015).

[19] S. M. Wu, J. Hoffman, J. E. Pearson, and A. Bhattacharya, Appl. Phys. Lett. **105**, 092409 (2014).

[20] N. Koon, Phys. Rev. Lett. **78**, 4865 (1997).

[21] A. E. Berkowitz and K. Takano, J. Magn. Magn. Mater. **200**, 552 (1999).

[22] S. Y. Huang, X. Fan, D. Qu, Y. P. Chen, W. G. Wang, J. Wu, T. Y. Chen, J. Q. Xiao, and C. L. Chien, Phys. Rev. Lett. **109**, 107204 (2012).

[23] Y. M. Lu, Y. Choi, C. M. Ortega, X. M. Cheng, J. W. Cai, S. Y. Huang, L. Sun, and C. L. Chien, Phys. Rev. Lett. **110**, 147207 (2013).

[24] Y. Pu, E. Johnston-Halperin, D. D. Awschalom, and J. Shi, Phys. Rev. Lett. **97**, 036601 (2006).

[25] A. D. Avery, M. R. Pufall, and B. L. Zink, Phys. Rev. Lett. **109**, 196602 (2012).

[26] T. Kimura, J. Hamrle, and Y. Otani, Phys. Rev. B **72**, 014461 (2005).

[27] H. L. Wang, C. H. Du, Y. Pu, R. Adur, P. C. Hammel, and F. Y. Yang, Phys. Rev. Lett. **112**, 197201 (2014).

[28] H. L. Wang, C. H. Du, P. C. Hammel, and F. Y. Yang, Appl. Phys. Lett. **104**, 202405 (2014).

[29] C. Du, H. Wang, F. Yang, and P. C. Hammel, Phys. Rev. B **90**, 140407(R) (2014).

[30] M. Morota, Y. Niimi, K. Ohnishi, D. H. Wei, T. Tanaka, H. Kontani, T. Kimura, and Y. Otani, Phys. Rev. B **83**, 174405 (2011).